CHAPTER 4
Forest Stand Height Estimation

Paul Siqueira, Professor of Electrical and Computer Engineering, Microwave Remote Sensing Laboratory, University of Massachusetts, Amherst

ABSTRACT

The measurement of forest structural characteristics is important for a variety of Monitoring, Reporting, and Verification (MRV) protocols in resource management. One characteristic of particular importance is Forest Stand Height (FSH), or the average height of trees in a forest stand. In this context, FSH can be used an indicator of the age of a forest stand, plant and animal habitats, and the amount of Above Ground Biomass (AGB) held in the forest stand. FSH can be measured through the use of terrestrial and/or airborne lidar, with airborne lidar being especially useful due to its wide area coverage and direct measurement of forest height. A difficulty with airborne measurements, however, is that while these measurements work well at the tens- to hundreds-of-hectares-level, they are difficult to scale beyond that.

One method for the spatial scaling of FSH is through the use of spaceborne Synthetic Aperture Radar (SAR), especially at L-band repeat-pass Interferometric SAR (InSAR), which can be obtained through repeat observations from ALOS-2 and the future NISAR mission. In this scenario, the measure of InSAR decorrelation can be related to FSH through the use of localized training data obtained from lidar. This chapter focuses on the use of repeat-pass InSAR for FSH estimation, and presents the theory, software, and examples of these methods. Although there is currently a limited availability of L-band SAR from ALOS-2, when NISAR launches in 2021, the presented method of FSH determination can be applied over large regions, especially when initialized using instruments such as the Global Ecosystems Dynamics Investigation Lidar (GEDI) aboard the International Space Station, or other lidar observations.

4.1 Theory

4.1.1 BACKGROUND AND BASIC CONCEPTS

The average height of trees in a forest stand, or Forest Stand Height (FSH), is an indicator of the age of a forest stand and an important forest structure metric that helps to characterize (1) plant and animal habitats, (2) the history of land use, and (3) the amount of Above Ground Biomass (AGB) held in the forest stand. The size of the forest stand in this context is minimally 1 ha in size, but is generally larger depending on the homogeneity of the forested region. In general, when using remote sensing data to estimate FSH, the smaller the size of the land unit, the less accurate the FSH estimate will be. This is due to basic sampling statistics and estimation errors that are incurred when a statistically varying quantity (such as forest height) is measured remotely.

4.1.1.1 Relating SAR to Forest Stand Height

SAR sensitivity to FSH is based on three fundamental SAR properties. These three fundamental properties are discussed below and are illustrated in **Figure 4.1**:

(1) As the number of scatterers increase within a SAR resolution cell, so does the reflected power. This trend is moderated by the effect of attenuation of signals as they pass through a forested canopy, and is directly related to the saturation effect seen in backscatter to biomass relationships (discussed in **Chapter 5**). Insomuch as the number of scatterers increases with FSH and forest density, observations of the backscatter power from radar can be used as an indirect measure of FSH. This relationship is often obtained through an empirical relationship between the two variables.

It should be noted that SAR data can have a number of different polarization combinations, with the simplest being a co-polarized return, such as HH or VV (see **Chapter 2**); followed by dual-polarized, which is a combination of one of the co-polarized returns with its cross-polarized counterpart (HH with HV, or VV with VH); and finally, the quad-polarized signature, which is the most complicated as it has all four components (HH, HV, VV, and VH) of the polarimetric scattering matrix. Because of the sensitivity of the cross-polarized signature to the multiple scattering that occurs in vegetated environments, the cross-polarized channels of the backscatter power are most often used for characterizing forest structure.

(2) In addition to the power measured in a SAR backscatter image, SAR can also very accurately measure the distance to targets. When the height of target is not accurately known, there exists an ambiguity in the geometric relationship between the target and the SAR sensor, principally through the look angle, which is defined as the angle between the nadir direction of the SAR and the vector pointing from the SAR to the target.

When two SAR observations are made, however, this angle can be determined very accurately through some basic trigonometric calculations and indeed can be used for measuring the topography of the Earth through a process known as Interferometric SAR, or InSAR. If the measure of InSAR height can be modeled relative to the bare ground surface, and if the topography of that surface can be determined through other means, then an estimate of the vegetation height can be determined by the difference between the InSAR-measured height and ground surface Digital Elevation Model (DEM).

In places where the topographic height is not well defined (e.g., in a forest canopy where the interferometrically measured height can mean either at the ground surface or the canopy top), a unique interferometric signature arises in which the detected height from the interferometer can be shown to be a random number. Its mean is an extinction weighted average of the radar signal penetration into the canopy. The term "extinction weighted average" refers to the loss of signal strength (extinction) as a radar signal penetrates a forest canopy. Hence, parts at the top of the canopy will contribute more to the backscatter signature than the bottom of the

canopy. This depth of penetration is proportional to the signal wavelength (24 cm for L-band and 5-cm for C-band) and the density of scatterers. For interferometric applications, the vertical distribution of scatterers plays a role in the overall signature, and hence the use of the term "extinction weighted average." The magnitude of this weighted average is known as the "interferometric coherence," a normalized value with a range between 0 and 1. InSAR sensitivity to FSH statistics have led to a number of approaches to be explored using spaceborne satellites (e.g., Treuhaft & Siqueira 2000, Cloude & Papathanassiou 2001).

(3) For InSAR to work well over vegetated surfaces in the previously described manner, it is important to make the SAR observations simultaneously, or as close together in time as possible. This is because if the observations are made at different times, the targets within a SAR resolution cell may have moved, and this movement will cause an error in measuring the trigonometric look angle and will create a reduction in the interferometric coherence. This process is known as "temporal decorrelation," that is, the more that a target changes between observations, the lower the coherence will be.

When an InSAR system makes both observations at the same time (typically requiring two satellites or a single airborne platform with two antennas), it is known as "single-pass InSAR." Conversely, if the observations of the scene are made at different times, this is called "repeat-pass InSAR."

One way FSH can be estimated from repeat-pass InSAR is to measure the amount of temporal decorrelation that has occurred between passes and to make the broad assumption that the taller a tree (or forest stand) is, the more movement that will occur between passes of the satellite. Hence, when the interferometric coherence is measured, it can indirectly (through an empirical relationship) be used to estimate FSH.

As in the case of backscatter to biomass relationships, the cross-polarized channel (HV) of the interferometric coherence is more sensitive to FSH that the co-polarized channels (HH and VV).

Based on the principles highlighted above, a set of algorithms has been created for estimating FSH from InSAR observations. Because most spaceborne SAR systems cannot perform single-pass interferometry, the FSH algorithm relies on the repeat-pass relationship between interferometric coherence and vegetation height.
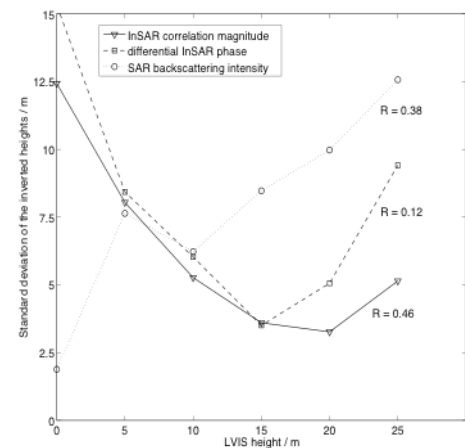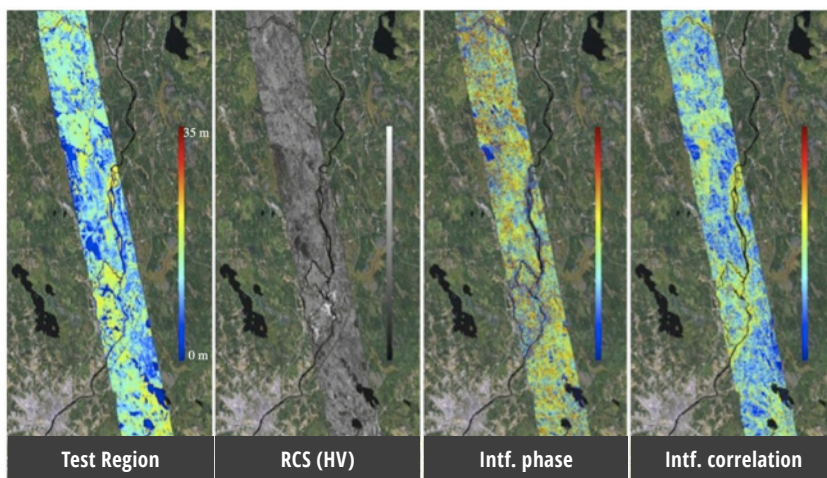

Figure 4.1 *Illustration of the three principles behind the relationship of SAR measurements to vegetation height. Shown from left to right are (a) a test region located in the U.S. state of Maine imaged by the LVIS lidar sensor, (b) the radar backscatter intensity for the region (grayscale), (c) the height difference between L-band repeat-pass SAR and the ground surface DEM, and (d) a height estimate based on the interferometric correlation. The graphic at the right (e) shows the FSH error relative to the lidar measurement for each of the three SAR methods derived from the cross-polarized signal. It can be seen from the plot that for vegetation heights of less than 10 m, the backscatter intensity is most accurate. For vegetation taller than 10 m, the InSAR coherence proves to be more accurate.*

4.1.1.2 Mission Platforms for Estimating Forest Stand Height

At the time of this writing, and algorithm development, for spaceborne applications with a global extent, there are only two SAR systems with single-pass interferometry. One of these is the Shuttle Radar Topography Mission (SRTM), a C-band InSAR flown on board NASA's space shuttle for an 11-day mission in February 2000. The other is TanDEM-X, flown by the German Space Agency (DLR), where data were collected by two co-orbiting satellites at X-band in 2010 and made mostly available through commercial arrangements. Because both satellites operate with wavelengths less than 10 cm, the signals from SRTM and TanDEM-X do not penetrate far into the canopy, and without a model for the ground surface DEM, will have difficulty estimating FSH.

Upon implementation, a significant source of error in estimating coherence is related to thermal noise. As the amount of backscatter power received from a target decreases, an increased proportion of the coherence measurement is related to the signal that remains. In the case of a radar system, the residual signal not originating from the target itself is considered thermal noise (or simply instrument noise). Since bare surfaces (especially smooth surfaces) do not have a strong backscatter signal, the error in measuring interferometric coherence is large. Hence, the error in FSH estimation increases with decreasing values of vegetation height. For this reason, the best estimate of FSH made from repeat-pass interferometry is made from a combination of SAR backscatter power and InSAR coherence. For this reason, the approach described here can be referred to as a combined SAR/InSAR estimation of FSH.

With respect to theory, a final note should be made about this method's sensitivity to the observing SAR's wavelength. For most terrestrial remote sensing systems, wavelengths range between ~1 m (P-band) to ~3 cm (X-band) (for more information on SAR wavelengths, see **Chapter 2, Section 2.3.1**). Because vegetation structures are on the order of some tens of centimeters, forest vegetation is often best observed using P- and L-bands (~24 cm). For L-band SAR, only the Japanese Aerospace Exploration

Agency's (JAXA's) JERS-1 and ALOS-1 and -2 satellites are available, but are limited due to their observing strategy and data distribution policy. The European Space Agency's (ESA's) Sentinel-1a and -1b satellites that operate at C-band (5 cm) are potential resources, but are limited for repeat-pass InSAR because of the short wavelength and dominance of temporal decorrelation over vegetated targets.

This leaves the capacity for estimating FSH on a global basis to future satellite systems. Of these, there are three upcoming missions that may fill this need:

(1) The Argentinian Space Agency's (CONAE's) L-band SAOCOM mission that was launched in 2018. The observing plan and data availability for this mission are currently not known.

(2) ESA's P-band Biomass mission, which will launch in the 2021–2022 timeframe. This will be a first-of-its-kind spaceborne P-band repeat-pass InSAR.

(3) NASA and the Indian Space Research Organization's (ISRO's) L-band and S-band (10 cm) NISAR mission, which will launch in late 2021 or early 2022. Data will be freely available and have global coverage at L-band.

With the NISAR mission in mind, and understanding the C-band wavelength limitations of ESA's Sentinel-1 data, prototyping of FSH algorithms have concentrated on L-band using geographically limited ALOS data as a proxy.

4.1.1.3 Additional Theoretical and Applied Background

To learn more about the FSH algorithm and to access Python-based scripts for executing the algorithms described here, refer to the following journal articles:

• An introductory paper on the topic:

Lei, Y., P. Siqueira, "Estimation of Forest Height Using Spaceborne Repeat-Pass L-Band InSAR Correlation Magnitude over the US State of Maine," Rem. Sens., 6(11), 10252-10285, 2014.

• An automated method for mosaicking FSH data and minimizing errors

Lei, Y., P. Siqueira, "An Automatic Mosaicking Algorithm for

the Generation of a Large-Scale Forest Height Map Using Spaceborne Repeat-Pass InSAR Correlation Magnitude," Rem. Sens., 7(5), 5639-5659, 2015.

• An article describing the theory behind the approach

Lei, Y., P. Siqueira, R. Treuhaft, "A physical scattering model of repeat-pass InSAR correlation for vegetation," Wvs. Rand. Cmpx. Med., 27(1), 129-152, 2017.

• Application of FSH and Repeat-pass InSAR for Forest disturbance detection

Lei, Y., R. Lucas, P. Siqueira, M. Schmidt, and R. Treuhaft, "Detection of forest disturbance with spaceborne repeat-pass SAR interferometry," IEEE Trans. Geosci. Rem. Sens., 56(4), 2424-2439, Apr 2018.

• Statistical evaluation of the FSH algorithm over a wide area

Lei, Y., P. Siqueira, N. Torbick, M. Ducey, D. Chowdhury, and W. Salas, "Generation of large-scale moderate-resolution forest height mosaic with spaceborne repeat-pass SAR interferometry and lidar," To be published IEEE Trans. Geosci. Rem. Sens., 34 pp., 2019.

4.1.2 PROCESSING TECHNIQUES

InSAR data processing for FSH estimation requires either raw satellite data that have been downlinked but not processed, or SAR data that have been processed into Single Look Complex (SLC) imagery that is appropriate for forming interferograms. If the user has access to SLCs directly, then it is recommended to begin from there. If only the raw data are available, then some additional processing is necessary. One advantage to beginning with raw data is that the output formats of the interferograms and ancillary data are assembled in such a way as to make it easy to follow-on the processing with additional steps implemented to estimate FSH.

Software for processing raw data into SLCs can be obtained both commercially and through open source licensing agreements. Of the open source licensing processors, there are two that have been used for processing raw ALOS data into SLCs and then into FSH estimates. These are ROI_PAC (Repeat Orbit Interfer-

ometry PACkage) and ISCE (InSAR Scientific Computing Environment). In this document, ROI_PAC is used because it has completed its development lifetime is and is somewhat easier to obtain than ISCE. At the time of this writing, ISCE continues to be developed, whereas ROI_PAC is not. With this in mind, the scripts that estimate FSH from SLCs have been designed to work with both ROI_PAC and ISCE.

It is important to note that while Python programs can be run in Windows, Mac OS X, and Unix environments, processing raw data into interferograms using the methods described requires a Unix or Linux environment. For this reason, it is assumed that the reader has access to these types of computing capabilities and is familiar with operating inside of them.

The following sections describe three steps: (1) downloading and processing ALOS data, (2) staging of ground validation data (necessary for establishing empirical relationships between SAR backscatter power and interferometric coherence to forest height), and (3) running the FSH algorithms. Users starting with SLC data may begin at the second step.

4.1.2.1 Processing ALOS Data

To understand SAR data processing for FSH estimation, it is helpful to refer to a particular software so that the user can conceptualize the steps necessary to process SAR data. This section begins with a short description on how to obtain and install the ROI_PAC software.

4.1.2.1.1 Installing and Testing ROI_PAC

In this work, the ROI_PAC processing software can be obtained in TGZ (i.e., gzipped TAR) format at http://www.openchannelfoundation.org/projects/ROI_PAC. To fully install the ROI_PAC software, it is also necessary to have available a Fortran compiler (e.g., gfortran) and the FFTW library. Additional details for the installation of ROI_PAC software can be found at http://roipac.org/cgi-bin/moin.cgi/Installation.

The ROI_PAC software distribution comes with a test dataset that can be processed by ROI_PAC to test the software installation. The details of this test processing can be found in the ROI_PAC installation subdirectory fullpath/contrib/multtest.sh, where fullpath refers to the folder that the ROI_PAC installation archive is unzipped.
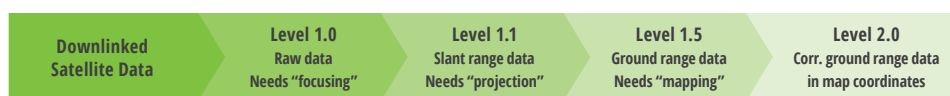

Figure 4.2 *Processing chain for SAR data showing the steps that occur in the transition of a SAR image from raw data into processed data. Interferometric analysis should be done at Level 1.1. Level 2.0 refers to data that have been multi-looked, corrected for terrain effects, etc. Level 3.0 data (not shown) refers to data that have been interpreted in some way, either through classification or parameter estimation. Note that the different level numbering specified in the headings of the processing steps may vary from space agency to space agency.*
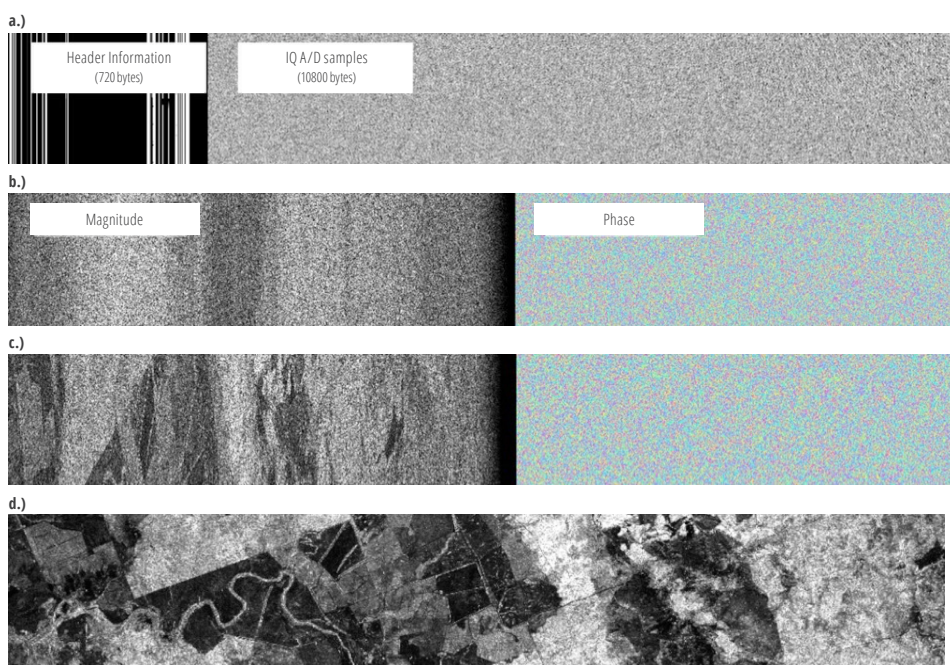

Figure 4.3 *The four steps of processing ALOS SAR data beginning from (a) raw samples from the satellite, (b) range compression, (c) azimuth compression resulting in an SLC, and (d) projection into map coordinates (Level 2.0). Shown in parts (b) and (c) is the signal phase used in interferometry for determining topographic height and coherence.*

4.1.2.1.2 SAR Processing

Processing SAR data from raw digital values retrieved from the satellite into what ultimately becomes SAR imagery can be a detailed and complex process. In the processing of SAR data, corrections are made to account for the motion of the satellite and for the image projection effects that arise from the atmosphere, viewing geometry, and topography of the Earth. A summary of the basic steps executed in processing are shown in **Figure 4.2**. An illustration of SAR data as they are processed from raw imagery into map-projected ground-range (i.e., Level 2.0) is shown in **Figure 4.3**.

4.1.2.2 Staging of Ground Validation Data

FSH ground validation data is an important component of the data processing methodology necessary for converting interferometric SAR data into FSH estimates. The FSH algorithms are implemented such that they can ingest geographically explicit data of measured (either ground-based or lidar) forest heights through the GeoTIFF format. The following subsection provides a review of the ground validation data necessary for the running of FSH.

4.1.2.2.1 Types of Ground Validation Input

There are two types of ancillary ground validation data that are necessary for completing the specification of the empirical models used for the estimation of FSH from SAR data: (1) a Forest/Non-Forest (FNF)

mask that indicates where in the image the estimates should be exercised, and (2) a map of locations where forest height has been previously determined and will be used by the FSH algorithm for the training of the empirical models.

The FNF map can be derived from a number of sources or created independently by the user. Examples of external data sources that can be used to derive an FNF mask are (1) JAXA's FNF mask, (2) the U.S. National LandCover Dataset (NLCD), and (3) ESA's CCI Landcover (formerly GlobCover). From datasets such as these, a determination can be made where forests are situated and hence, where it is desired to estimate FSH. The contents of the FNF mask should be such that all regions where FSH should be estimated have a value of 0, and all regions where FSH should not be estimated have a value of 1. An example of this classification is shown in **Figure 4.4(a)**.

4.1.2.2.2 Use of Lidar for Forest Stand Height Model Development

To determine values for the empirical models that relate radar backscatter power and interferometric coherence to FSH, some independent measure of forest height is necessary. Because of its ability to acquire accurate measurements of vegetation height over an extended geographic region, lidar is a preferred method for determining the coefficients that parameterize these models. An example of lidar data for a region in Maine, U.S., is shown in **Figure 4.4(b)**, which was derived from the Laser Vegetation Imaging Sensor (LVIS) operated by NASA's Goddard Space Flight Center.

The LVIS data in **Figure 4.4** show vegetation height gridded into 30-m pixels, converted into a GeoTIFF format, and visualized using QGIS software. A resolution of 30 m was selected for this example because it is commensurate with the LVIS spot size of 25 m and the multi-looked resolution of the L-band SAR data. An example of the distribution of LVIS-estimated tree heights is shown in **Figure 4.5**.

4.1.2.2.3 Alternative Methods for Estimating Forest Height

If lidar data are not available, then another form of independent forest height measurement over the training area needs to be identified or created. Since
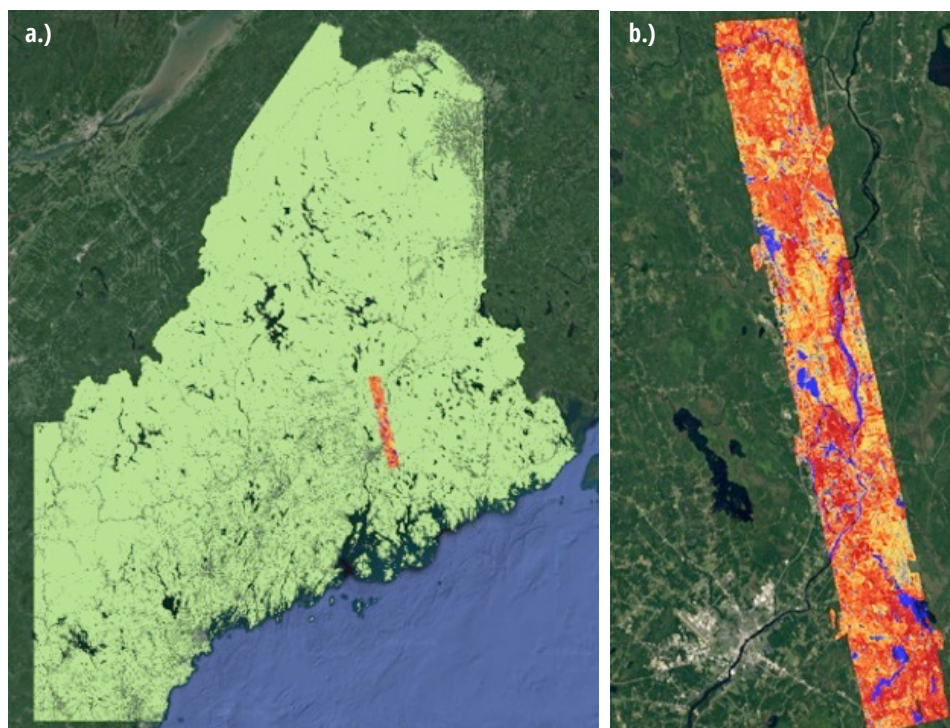

Figure 4.4 *Examples of ground validation input for the FSH algorithm: (a) Optical image overlain with the FNF mask (green areas indicate regions that will be estimated for FSH), and (b) image of Laser Vegetation Imaging Sensor- (LVIS-) derived vegetation height, where blue indicates zero height, and dark red indicates the maximum height of 25 m. Data such as these are used for determining coefficients for the empirical models that relate the radar backscatter and interferometric coherence to vegetation height.*
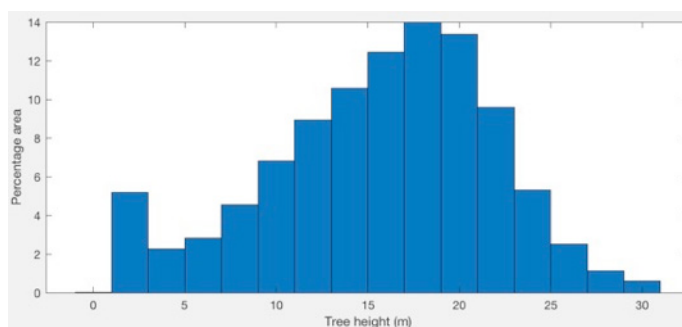

Figure 4.5 *Histogram of lidar-derived tree heights used for the training of empirical models of FSH. The spatial resolution of the LVIS data used here is 30 m.*

the FSH estimator is only accurate to the 3- to 5-m level, a simple solution would be to perform a land-cover classification of a region using optical data. Stands of different ages and species composition will have different heights, which can be estimated from the ground to the same accuracy as the FSH. During the development and testing of the FSH algorithm described here, this approach was used at times. However, the results have been somewhat mixed in terms of success.

As a final approach, it should be noted that freely available satellite resources of lidar data are either available or soon to become available. Notable among these are ICESAT-1 and -2, as well as the upcoming NASA GEDI mission.

4.1.2.3 Running Forest Stand Height Algorithms

In order to run the FSH algorithms, it is assumed that the first two steps of the process described in **Section 4.1.2** have been accomplished: (1) the creation or obtaining of SLCs and (2) the obtaining of an FNF mask and vegetation height ground validation data. Once these

two steps have been accomplished, the data should be organized in a file structure such that individual folders hold results from individual interferograms between two dates (the SLCs and ancillary data for individual scenes (frames) and orbit (path) numbers). For any one frame and path number, there may exist multiple interferograms, related to multiple repeat-pass combinations of data from two different dates. These interferograms should be stored in subdirectories with the naming convention: `int_date1_date2`. Scenes from differing frames and paths can be interferometrically processed in order to create an estimate of FSH over an extended geographic region.

The interferogram subdirectories will hold all of the data and information necessary for creating and documenting interferograms made for an observation on two specific dates (date1 and date2). For ROI_PAC-processed data, the most important file looks like `geo_date1-date2_2rlks.cor` and `geo_date1-date2_2rlks.cor.rsc`. The resource (".rsc") file is a text file that has information on the location and size of the geolocated correlation data held in `geo_date1-date2_2rlks.cor`. The format of the correlation file is known as "sample-interleaved," or an RMG format file. An image of interferometric coherence (color) overlain on a geo-referenced image of radar backscatter cross-polarized power is shown in **Figure 4.6**.

Because radar data is organized in terms of orbits and scenes, in order to make a map of FSH over an extended geographic region, it is necessary to mosaic the images. While the process of mosaicking can be done either before or after the estimation of FSH, it is best to do so beforehand to take advantage of the overlap region between images in adjacent paths. In these regions, while the value of the coherence magnitude may vary due to the fact that the observations (and image pairs) have occurred from different orbits (and hence different dates), the overlap regions can be used to correct for these temporal differences and to adjust the coefficients for the empirical relationships of the SAR products to estimates of FSH. An example of this process is shown in **Figure 4.7**.

Once the data have been organized into directories of scenes described by their individual row and path numbers, and the interferograms have been examined
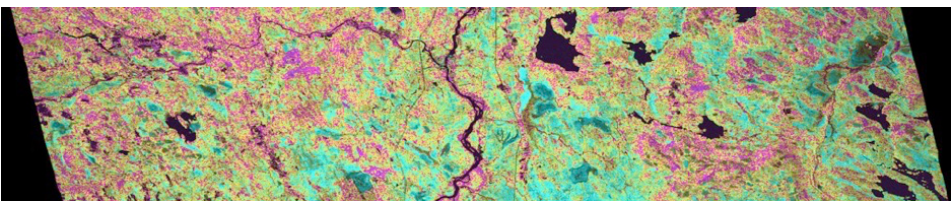

Figure 4.6 *A combined image of interferometric coherence (color) and cross-polarized backscatter power (brightness). The interferometric coherence in this image ranges between 0.1 (magenta) and 0.6 (cyan). Regions of low interferometric coherence are likely due to the presence of vegetation.*
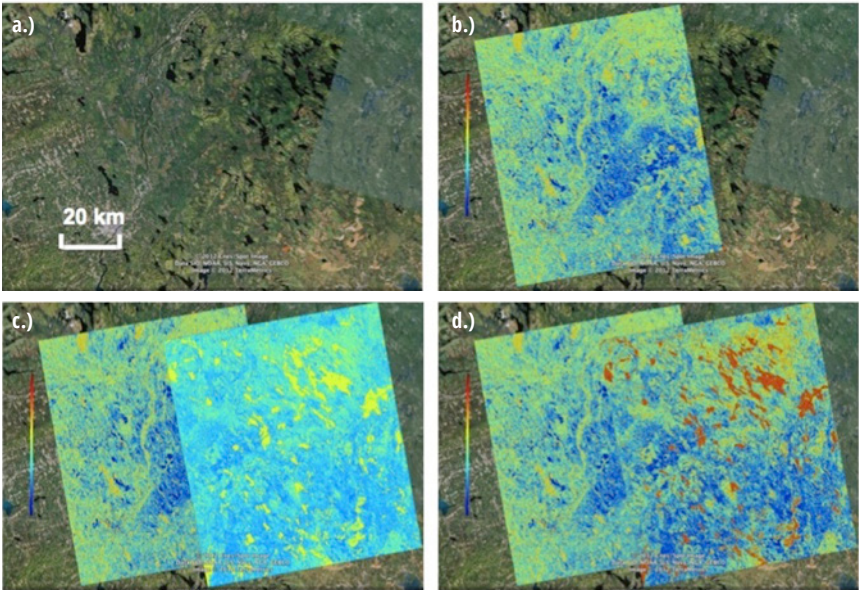

Figure 4.7 *Example of FSH/coherence equalization through the use of overlapping image regions: (a) optical image in central Maine, (b) an estimate of FSH for this region (color scale on the left extends from blue (0 m) to red (35 m)) where lidar data were available from LVIS, (c) an unconstrained estimate of FSH from an adjacent satellite pass, and (d) a corrected estimate of FSH for both scenes included in the mosaic. Color scale for all figures is the same (from Lei & Siqueira 2014).*

to determine which SLC pairs yield data with the highest coherence (i.e., the least amount of temporal decorrelation), there remains the task of creating what is known as a "flag file" and a "link file."

In this context, the *flag file* is a listing of all of the interferograms to be used in creating the region-wide mosaic of FSH. In the case discussed here, there are three such row/path combinations that will create a three-scene mosaic of FSH located in central Maine. The middle of the three scenes overlaps with the LVIS data discussed in **Section 4.1.2**, and all scenes are within

the region where identification of FNF is used for determining geographic locations where the FSH algorithm will be applied. An example of the contents of a flag file (in text format) is at the bottom of the page:

In this example, the first column of numbers indicates the interferogram number, the second column is the root file name of the data that forms the interferogram, the third and fourth columns are the dates that the data were collected for the interferometric pairs, the fifth and sixth columns give the satellite path and orbit numbers (respectively), and the last

001	890_120_20070727_HV_20070911_HV	070727	070911	890	120	HV
002	890_119_20070710_HV_20071010_HV	070710	071010	890	119	HV
003	890_118_20070808_HV_20070923_HV	070808	070923	890	118	HV

column indicates the polarization of the data.

A question that may arise when looking at the flag file is if it is possible to use other polarization combinations (e.g., HH and/or VV) for the determination of FSH. Indeed, such combinations were tested in the development stages of the algorithm, and it was determined that cross-polarized data worked best because of its higher sensitivity to volume scattering than co-polarized data. Similarly, other polarization combinations that emphasize the volume scattering return over surface scattering components (such as the circular polarization combination of LR) would be equally appropriate for the algorithm. If only co-polarized data are available, however, then it is generally preferable to have HH-polarization over VV, and then to move forward with the FSH algorithm, with the expectation that both accuracy and sensitivity will be reduced.

The *link file* mentioned above provides information on which files are expected to have some degree of geographic overlap and hence be used in propagating the coefficients of FSH. While many files may have such a geographic overlap—and that, indeed, this overlap can be automatically calculated—a separate link file is desired so that links can be added or broken as necessary in order to account for the varying quality of data in the overlap region used to estimate the coefficients (e.g., a scene with a particularly high degree of temporal decorrelation can be removed from the link list). A simple example of the text-formatted link file is as follows:

<div align="center">

2   1

2   3

</div>

This indicates that image 2 is connected to image 1, and that image 2 is also connected to image 3 (and also that images 1 and 3 are not connected).

In this context, the high degree of temporal decorrelation referenced in the previous paragraph indicates those situations in which the temporal decorrelation is large enough to obliterate any information content in the repeat-pass interferogram. Such is the case when the average interferometric correlation magnitude for a scene falls in the range of 0 to 0.5.

Once these files are created and put into place, the FSH set of scripts can be run by calling it in the command line and passing arguments that indicate the

various input file names as well as ancillary information. An example of a call to the FSH algorithm call is

```
python forest_stand_height.py <#
scenes> <# edges> <start scene #>
<# iterations> <link filename> <flag
filename> <lidar heights file>
<forest/non-forest file> <directory
of input/output files>
<list of output formats>

--flag_proc=0
```

In the last line of the FSH algorithm call, the list of output formats should be in quotes, and can contain one or all of the following: "`tif kml gif mat json`". In other words, output formats can be created for any of these options. Further, the command option `--flag_proc 0` indicates that the input data has been processed into SLCs by the ROI_PAC algorithm (as opposed to processing by ISCE, which should have a value of 1 instead).

4.1.3 ALGORITHM DEVELOPMENT

The FSH algorithm described in **Sections 4.1.1 and 4.1.2** are based on a combination of empirical relationships between cross-polarized radar backscatter power and interferometric coherence. Through the development of the algorithm, and following analysis such as that shown in **Figure 4.1**, it has been determined that FSH values below 10 m should be determined by the backscatter power relationship, and values above this threshold should be determined by interferometric coherence. In order to determine if this threshold has been met, the interferometric coherence version of FSH is first computed, and in regions where that is determined to be below the threshold value, the backscatter power empirical relationship is used.

A block diagram for this approach is given in **Figure 4.8**. In the diagram, parallelograms refer to inputs and outputs of the algorithm. Rectangles are steps in the processing, and a diamond is a point of evaluation. Also, in the diagram, the variable h_v refers to the value of FSH, and $\rho = [S_{scene} \quad C_{scene}]$ is the set of two values per scene that parameterize the model that relates temporal decorrelation to the vegetation height (**Sec. 4.1.3.2**) (see Lei et al. 2019).

In order to gain some appreciation of the simplicity of the relationships described above, it is valuable to specify what these equations are. A more detailed ex-
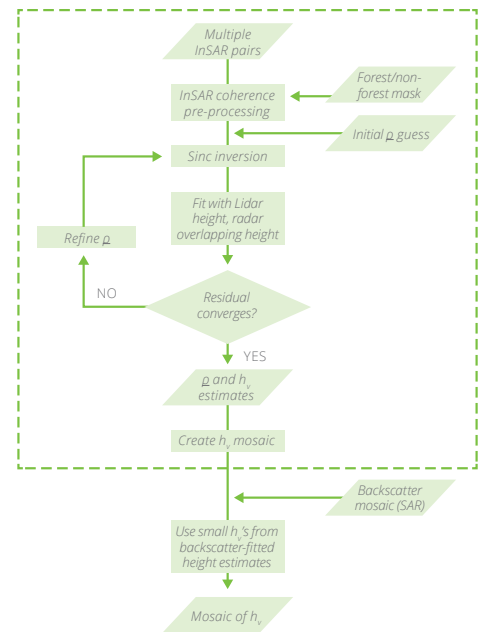

Figure 4.8 *Block diagram for the processing of FSH.*

planation of this approach, complete with equations and a statistical examination, can be found in Lei et al. (2019).

4.1.3.1 Relationship of Backscatter to Forest Stand Height

The backscatter power, after correcting for topographic and other geometric effects, is written as

$$\gamma^0 = A\left(1 - e^{-Bh_v^C}\right), \qquad (4.1)$$

where γ^0 is the terrain-corrected form of radar cross section (e.g., see Small 2011), h_v is the vegetation height, and the coefficients A, B, and C are determined in the FSH algorithm using a least-squares fit between the backscatter power and the vegetation height provided by the ground validation and/or overlap data between scenes. Sample values for these coefficients that have been automatically determined by the FSH algorithm are $A = 0.11$, $B = 0.0622$, and $C = 1.0143$.

A common issue with the relationship of backscatter to vegetation characteristics is that above a certain threshold of biomass, there is no longer a sensitivity of increasing γ^0 to increasing biomass. This saturation effect is wavelength-dependent. At L-band, an accepted value for the saturation limit is for 100 tons of biomass/hectare. Under the assumption that a rela-

tionship exists between vegetation height and biomass, whatever that may be, there is a similar saturation effect that occurs between γ^0 and h_v. This is reflected in the exponential relationship shown at the beginning of this section. While the saturation limits of sensitivity of γ^0 to h_v are less well-characterized, nominal estimates for these values provided in **Table 4.1**.

Note that values listed in the table are nominal values only and are strongly dependent on the biome, stand age, soil moisture and surface roughness.

When working in a specific region, however, the *correct approach* for determining these limits is to make a plot of radar backscatter as a function of lidar-derived vegetation heights.

In this section, backscatter power is referred to as γ^0. This backscatter power is a measure of the power that the radar receives from a particular region on the Earth's surface that is reflecting energy back to the radar. These values are stored on the satellite or airborne platform in digital values that are related to the power recorded by the radar. After processing to put the data into ground coordinates, and to perform aperture synthesis (a critical part of SAR processing), these values are transformed by the processor and provided to the user either as Digital Numbers (DN values) or in terms of calibrated radar backscatter power, either in units of σ^0 or γ^0, depending on the level of processing employed. The term "calibration" refers to correcting the radar power returns for gains that are internal to the radar system and processing chain and making all measurements proportional to the transmitted power. Values of σ^0 are calibrated in terms of the range coordinate of the radar system and have been normalized for the size of the area reflecting the energy back to the system (larger areas will reflect more energy). The units of σ^0 are in m^2/m^2. The radar cross section σ is not normalized for this area and is in units of m^2. When a DEM is used and the value of the radar cross section is adjusted to account for the intercepted surface area in the direction of radar viewing, this is what is termed γ^0 and is the form of radar cross section most appropriate for quantitative analysis (Small 2011).

4.1.3.2 Relationship of Interferometric Coherence to Forest Stand Height

The interferometric coherence is derived from

BAND	WAVELENGTH	FSH	HV BACKSCATTER SATURATION LEVEL
X- (10 GHz)	3 cm	10 cm	-10 dB
C- (5.4 Ghz)	5.6 cm	1 m	-12 dB
L- (1.2 GHz)	24 cm	10 m	-13 dB

Table 4.1 *Nominal estimates for HV backscatter saturation levels for typical SAR wavelengths.*

the interferometric correlation, which is the normalized geometric average between two complex images. Mathematically, the interferometric correlation γ is defined as

$$\gamma = \frac{\langle E_1 E_2^* \rangle}{\sqrt{\langle |E_1|^2 \rangle \langle |E_2|^2 \rangle}} \, , \qquad (4.2)$$

where E_1 and E_2 are the complex values of radar cross sections observed by the SAR satellite and delivered as SLCs, the brackets indicate averaging over multiple looks, and * indicates a complex conjugation. Note that the γ defined in the interferometric correlation expression above is not the same as the γ^0 specified for the terrain-corrected value of radar cross section described in **Section 4.1.3.1**. When an image is referred to as an interferogram, it indicates an image of γ as specified previously. This correlation is complex-valued, with its magnitude (the coherence) varying between 0 and 1, and the phase between 0 and 2π. A signal with low correlation will have a coherence close to 0 and a random phase. A signal with a high correlation will have a coherence close to 1 and a well-determined phase that is related to the viewing geometry.

A number of factors contribute to the general value of the interferometric correlation:

- The geometric correlation due to incidence angle and projection effects, γ_{geom}
- The correlation related the proportion of noise in the receive system, γ_{SNR}
- The correlation related to the interferometric baseline and the volume scattering of the target, γ_{vol}
- The temporal correlation (or decorrelation, as the case may be), γ_{temp}

The net effect of all of these sources of decorrelation multiplied by one another make up the total observed correlation γ as described previously by

Eq. (4.2):

$$\gamma = \gamma_{geom} \cdot \gamma_{SNR} \cdot \gamma_{vol} \cdot \gamma_{temp} \, . \qquad (4.3)$$

When a satellite doing repeat-pass interferometry and has an orbital repeat that minimizes the orbital distance between repeat-orbits, the condition exists known as "zero-baseline interferometry," which is the case for most repeat-pass SAR systems. In such cases, the contribution of the volumetric decorrelation γ_{vol} to the total correlation is minimal; hence, the best way for relating interferometric correlation to FSH is through the temporal decorrelation signature, which is a statistical-empirical relationship by its nature.

In the FSH algorithm, the combination of volume and temporal correlation (or coherence), $|\gamma_{v\&t}| = |\gamma_{vol}\gamma_{temp}|$, is related to the vegetation height h_v by the empirical equation:

$$\left| \gamma_{v\&t} \right| = S_{scene} \cdot sinc\left(\frac{h_v}{C_{scene}} \right) \, , \qquad (4.4)$$

where the coefficients of S_{scene} and C_{scene} are scene-wide coefficients (i.e., have only one value for the entire radar scene) determined using a least-squares fit to the ground validation data and/or overlap regions between neighboring interferograms (e.g., Lei et al. 2019). Typical
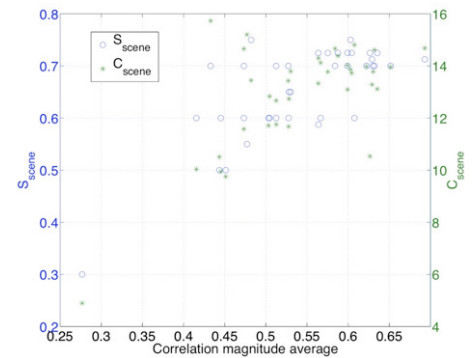

Figure 4.9 *Typical values for the model coefficients of S_{scene} and C_{scene} used by the FSH algorithm for relating vegetation height to the interferometric coherence.*
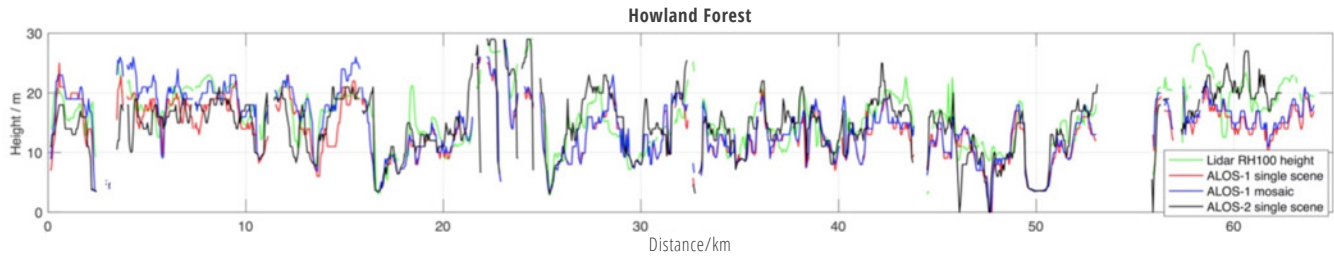
Figure 4.10 *A spatial comparison between lidar-derived tree height (RH100) from NASA's LVIS instrument, and the FSH approach using either the ALOS-1 or -2 sensors.*

values of S_{scene} and C_{scene} as determined in a 37-scene, statewide mosaic of FSH for Maine are shown in **Figure 4.9**. Note that values of S_{scene} and C_{scene} vary due to differing weather and soil moisture conditions that happen throughout the year and observing period of repeat-pass interferometry.

Once the coefficients for the empirical relationship between h_v and $|\gamma_{v\&t}|$ have been established, it is a simple matter to invert the relationship (using a lookup table or otherwise) to determine FSH over an extended region.

4.1.4 ACCURACY OF FINAL MEASUREMENTS

The accuracy of the estimates of FSH obtained using the methods described above is a subject of continued study. One example of the accuracy assessment is shown in **Figure 4.1**, which shows values for the Root-Mean-Square Error (RMSE) (residual) error of estimating FSH when compared to lidar data. In these cases, the error for FSH is 3.8 m when measured at a resolution of 400 x 800 m (32 ha) and using the interferometric correlation alone (i.e., not including the estimation improvement when backscatter power is used to estimate FSH for values of FSH < 10 m). When data from the coherence are combined with the backscatter power, the estimated error is better than 3.5 m when measured at a resolution of 6 ha, an improvement of more than four times.

Factors that affect the accuracy of the FSH algorithm are:

- The degree that temporal conditions affect the interferometric coherence
- The availability of SAR data at wavelengths of L-band (or P-band; C-band data from Sentinel-1a for instance, is not appropriate for FSH determination using these methods)
- Availability and quality of ground validation data

Figure 4.11 *A qualitative comparison of (a) lidar-derived vegetation height from the GRANIT sensor and (b) SAR-derived FSH for a site that is more than 300 km away from the location where the LVIS lidar was used for determining the model coefficients. The 6-ha RMSE between the two measures of FSH is 3.9 m (from Lei et al. 2019)*

that can be used for determining model coefficients

- The spatial dimension (area) that the accuracy is being assessed.

With respect to this last parameter that affects accuracy, for many remote sensing applications, so long as there are no biases in the data, resolution can be traded for accuracy. In the case of the FSH algorithm, the accuracy is quoted to be 3.5 m at a 6-ha resolution. To determine the accuracy of the algorithm at a 1-ha resolution, the reporting requirement for REDD+ MRV (see **Section 4.1.7**), the extrapolated accuracy would be $\sqrt{6\ ha/1\ ha} \times 3.5\ m = 8.6\ m$.

An example of a wide-area application of the FSH algorithm can be found in Lei et al. 2019, with some of the salient results shown in **Figure 4.10**.

A simple method of assessment is to show a spatial comparison between lidar-derived heights and those obtained from the FSH algorithm. For a transect extracted from the LVIS data shown in **Figure 4.4** over the Howland forest in Maine, a comparison is made in **Figure 4.9** between the lidar-derived height and the height determined from the InSAR and SAR backscat-
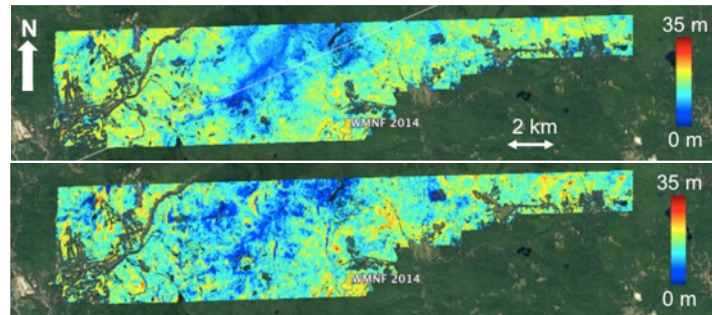
ter power algorithm discussed here. The plot shows excellent agreement between the two measures, but may be unsurprising in that the lidar data were used to calibrate the scene-wide coefficients used by the SAR/InSAR FSH algorithm for estimating height.

A better comparison can be assessed by finding a nearby region that is also sampled by lidar but not used in determining the model coefficients. Such a site exists in the White Mountain National Forest (WMNF) in eastern New Hampshire, U.S., more than 300 km away and distant from the originally trained SAR/InSAR scene by 5 orbits (and equivalently, at least 5 scenes). By using the overlap regions between adjacent passes of the satellite, the coefficients determined from the Howland Forest can be propagated to the WMNF scenes and then compared to the lidar data that are available there. This is shown in **Figure 4.11** in a qualitative sense. Quantitatively, the residual differences between the two datasets have a standard deviation of 3.9 m when measured at a resolution of 6 ha.

A final comparison can be made for forest heights assessed at the county level, as shown in **Figure 4.12**. In this case, data from the U.S. Forest Service's
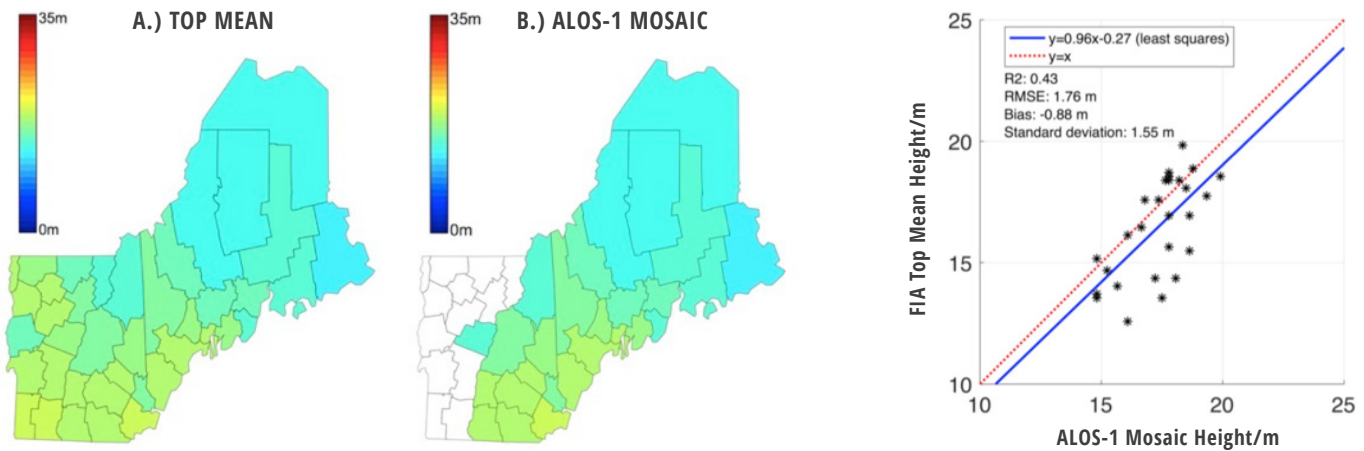
Figure 4.12 Comparison of county-level assessments of vegetation height obtained (a) by the U.S. Forest Service using FIA plots and (b) those obtained using the FSH algorithm. At right is a quantitative comparison between the two datasets.

Field Inventory Analysis (FIA) program is used for creating an independent assessment of forest height for each county in the region (see Lei et al. 2019). When these county-level estimates are compared with the SAR/InSAR estimates of FSH at the same scale, the RMSE is measured to be 1.8 m, as shown in the figure.

In general, as shown in **Figure 4.11**, the differences between independently derived measures of forest height and those determined using the SAR/InSAR algorithm for FSH compare very well and have residual errors on the order of 4 m for map resolutions of 6 ha. Under the assumption that the independently derived estimates of FSH are more accurate than the SAR/InSAR approach, the dominant contributor to this residual error is due to *model error* related to the difficulty in capturing the effect of weather events on the InSAR signature. One way to overcome this type of error is for the repeat-pass observations to take place over shorter timescales than the 46-day repeat period of ALOS-1. Initial studies using ALOS-2 data (that has a 14-day repeat period) have shown that, indeed, the error is reduced. The observing plan and data distribution policies of ALOS-2, however, have not enabled a fuller assessment that could be applied over a region as large as that shown in **Figure 4.4**, and so opportune datasets where the algorithm can be further tested remain to be found.

4.1.5 SOURCES OF ERROR

After presenting the SAR/InSAR algorithm for deter-

mining FSH in **Sections 4.1.1–4.1.4**, it is important to summarize the different sources of error that can confound this measurement. These sources of error are:

- **Spatially varying degree of temporal decorrelation**—The empirical models that relate SAR backscatter power and InSAR coherence to FSH described in **Section 4.1.3** rely on coefficients that are determined on a scene-wide basis (one radar scene or interferometric pair at a time). When weather affects the temporal signature on the radar imagery in a spatially varying manner within a single scene, then the scene-wide coefficients determined for the model, while correct in an average sense, will have a spatially varying error within the scene. This error can be improved by fitting the empirical models to the residual spatial variation. Such a fit would depend on the availability of ancillary data (e.g., lidar or ground validation) and would require a considerable amount of care during the fitting stage; hence, this is generally not done. A simpler approach to dealing with this type of error source would be to discard the data that suffer from this effect and substitute with data collected during a different time period.
- **Regions that are undergoing significant landcover change**—The InSAR component of the FSH algorithm relies on the temporal decorrelation signature to estimate vegetation height. When temporal decorrelation is due to causes other than the motion of vegetation proportion to

their height, an error in the estimation of FSH will occur. An example of such error can occur in agricultural regions, where the degree of change in the landcover and field management is high. Such locations show a high degree of temporal decorrelation and hence will be evaluated by the FSH algorithm as having tall forest stands. Similarly, urban areas and regions of open water and flooded areas will also display high degrees of temporal decorrelation that will cause difficulties for the FSH algorithm. A simple approach to dealing with this type of error source is to use a landcover classification converted to an FNF map that eliminates these regions from the estimation process.

- **Regions undergoing selective logging and clearcutting**—Similar to the error sources indicated above, regions undergoing selective logging and clearcutting will display a high degree of temporal decorrelation, and the estimation process will indicate unrealistically large values of FSH (40 m and taller in regions where such tree heights are not common). In these cases, an additional post-estimation step should be exercised to identify all of those regions estimated to have a large value of FSH by the algorithm, evaluate them independently to determine the cause (using optical data or otherwise), and flag the regions as being disturbed.
- **Topographic effects**—The InSAR portion of the FSH algorithm works best when the interfer-

ometric baseline is as close to zero as possible. For this reason, the algorithm is not subject to significant topographic relief. In regions of large topographic variation, the degree of layover and shadow is spatially varying and hence should be accounted for in the assessment. One way of correcting for topographic effects is to collect the data from different aspect angles, such as can be done between ascending and descending passes of the satellite. Once an evaluation has been made as to which regions have errors associated with the viewing geometry, these errors can be minimized by combining the results from the different orbital directions of the satellite.

4.1.6 COMBINATION WITH OPTICAL DATASETS

The SAR/InSAR method for estimating FSH lends itself very well to combining with optical datasets, whether active (lidar) or passive (e.g., Landsat, MODIS and Sentinel-2). In general, both serve important roles in the estimation of FSH. As explained in **Section 4.1.2**, lidar is important in the determination of model coefficients, and optical data are often used for creating landcover classification products to derive forest cover maps. These maps are then used to determine regions where the FSH algorithm should be exercised.

After calculating FSH using the algorithms detailed here, optical data (especially lidar (as shown in **Fig. 4.11**)) can serve the role of validation, an important component of the MRV system necessary for monitoring natural resources within a county's borders and meeting various United Nations agreements with developing countries.

4.1.7 MRV SYSTEMS IN THE CONTEXT OF REDD+

The United Nations Framework Convention on Climate Change (UNFCCC) describes the need for Measurement, Report, and Verification (MRV) of forest carbon stocks, implemented through the Reducing Emissions from Deforestation and Forest Degradation in Developing Countries (REDD+) program. This program seeks methods for independently verifying the status and change of carbon stocks within developing countries, especially as they undergo varying economic, population, and climate challenges.

The methods described here, especially as demonstrated in **Figure 4.11**, can be used for addressing this MRV need. Although in the context of this treatment, the methods have been demonstrated for an 11.6-million-ha region in the northeastern U.S., the same methods can be applied elsewhere in the world. What is required to achieve this reach are (1) the availability of repeat-pass L- or P-band SAR data, (2) an assessment of the regions where the FSH algorithms would be applied (e.g., a global/regional landcover map), and (3) the collection of ground validation or lidar data over regions near where the estimation of FSH would be applied.

4.1.8 LOOKING AHEAD

In recent years, the availability of spaceborne remote sensing data—both in terms of data distribution policy and collection of the data—has been expanding considerably. Along with this expanded availability has been an increasing need to apply these assets to better monitor natural resources on a global basis. Such monitoring is important for understanding the effects of climate, public policy, and population pressure on a changing environment.

Through the launching of NASA's GEDI and NISAR missions in 2018 and 2021, respectively, the monitoring of forest structure and FSH through the approach discussed here is well-positioned to address these needs. **Figure 4.13** illustrates how this can be accomplished using the side-looking mapping capability of NISAR and the nadir-looking sampling measures of vegetation height that will come from GEDI. The figure also shows how GEDI's 14-beam lidar samples will overlap the NISAR data, which will have a 250-km swath, a 12-day repeat period, and operate at L-band.

The baseline NISAR mission will create interferograms over most of the Earth's landcover surface every 12 days at dual-polarization. In this scenario, the cross-polarized (HV) interferometric coherence and backscatter power from NISAR will be compared with forest heights measured from GEDI and used to calculate the coefficients that parameterize the empirical equations described in **Section 4.1.3**. Even though the two missions may not be operating concurrently, the degree of change in the world forests will not be so large as to adversely affect the model parameterization.
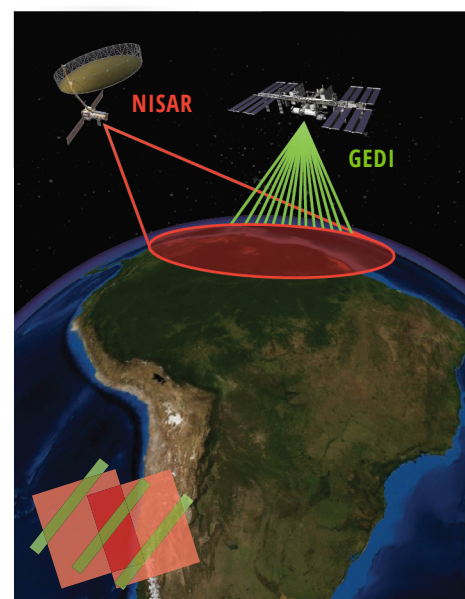
Prior to the availability of data from these two mis-

Figure 4.13 *Illustration on how NISAR and GEDI data can be combined to create a global estimate of FSH using the algorithms described here. Viewing geometries of NISAR and GEDI are displayed, along with an inset overlap schematic of NISAR data (red) with GEDI 14-beam lidar data (green) (Lei et al., 2019).*

sions, there are in principal sufficient resources from JAXA's ALOS-1 and -2 satellites as well as CONAE's SAOCOM satellite that can be combined with airborne lidar for obtaining results similar to those presented here and in published papers. The largest caveat at present is the availability of L-band SAR data, which is fairly restricted due to governmental policies, especially in the distribution of raw data. The larger scientific community, consisting of ecosystem and other Earth scientists, have been lobbying the governmental agencies of Japan and Argentina to free up some of these resources, however, and hence there is hope that some of these data will become more available, especially over the countries where the assessment and monitoring of forest resources with remote sensing data are critically important.

4.2 Python Scripts

A GitHub website with Python scripts written by Y. Lei, the principal developer of the FSH technique, has been set up. These scripts can be freely downloaded, along with an example-driven tutorial on the process, at https://github.com/leiyangleon/FSH.

4.3 References

Cloude, S. R. R., & Papathanassiou, K. P. P. (2001). Single-baseline polarimetric SAR interferometry. *IEEE Transactions on Geoscience and Remote Sensing, 39*(11), 2352–2363. http://doi.org/10.1109/36.964971

Lei, Y., & Siqueira, P. (2014). Estimation of forest height using spaceborne repeat-pass L-band InSAR correlation magnitude over the US state of Maine. *Remote Sensing, 6*(11), 10252–10285. http://doi.org/10.3390/rs61110252

Lei, Y., & Siqueira, P. (2015). An automatic mosaicking algorithm for the generation of a large-scale forest height map using spaceborne repeat-pass InSAR correlation magnitude. *Remote Sensing, 7*(5), 5639–5659. http://doi.org/10.3390/rs70505639

Lei, Y., Siqueira, P., Torbick, N., Ducey, M., Chowdhury, D., & Salas, W. (2019). Generation of large-scale moderate-resolution forest height mosaic with spaceborne repeat-pass SAR interferometry and lidar. *IEEE Transactions on Geoscience and Remote Sensing, 57*(2), 770–787. http://doi.org/10.1109/TGRS.2018.2860590

Lei, Y., Lucas, R., Siqueira, P., Schmidt, M., & Treuhaft, R. (2018). Detection of forest disturbance with spaceborne repeat-pass SAR interferometry. *IEEE Transactions on Geoscience and Remote Sensing, 56*(4), 2424–2439. http://doi.org/10.1109/TGRS.2017.2780158

Small, D., (2011) "Flattening gamma: Radiometric terrain correction for SAR imagery" *IEEE Transactions on Geoscience and Remote Sensing 49*(8), 3081-3093

Treuhaft, R. N., Siqueira, P. R. (2000). Vertical structure of vegetated land surfaces from interferometric and polarimetric radar. *Radio Science 35*, 141–177. https://doi.org/10.1029/1999RS900108

DR. PAUL SIQUEIRA is a Professor of Electrical and Computer Engineering at the University of Massachusetts in Amherst and is a co-Director of the Microwave Remote Sensing Laboratory, which has a long history in the development of Microwave Remote Sensing instrumentation for Earth Science Applications. Professor Siqueira is the Ecosystems Lead for the US NISAR mission, a joint project between NASA and the Indian Research Organization. Professor Siqueira has over 20 years experience in the use of SAR, has been a visiting scientist at the European Commission's Joint Research Center, was as a Senior Engineer at NASA's Jet Propulsion Laboratory and held a Bullard Fellowship at the Harvard Forest.